Phase relationships, and the structural, magnetic, and thermodynamic properties in the $Sm_5Si_xGe_{4-x}$ pseudobinary system

Kyunghan Ahn, V. K. Pecharsky, and K. A. Gschneidner, Jr.
Ames Laboratory, Iowa State University, Ames, Iowa 50011-3020, USA and Department of Materials Science and Engineering, Iowa State University, Ames, Iowa 50011-2300, USA

(Received 15 March 2007; revised manuscript received 25 April 2007; published 12 July 2007)

The crystallography, phase relationships, and physical properties of the $Sm_5Si_xGe_{4-x}$ alloys with $0 \leqslant x \leqslant 4$ have been investigated by using x-ray powder diffraction, dc magnetization, and heat capacity measurements between ~3 K and 350 K in magnetic fields ranging from 0 and 10 T. Similar to $Gd_5Si_xGe_{4-x}$, there are three distinct phase regions in the $Sm_5Si_xGe_{4-x}$ system: the Gd_5Si_4 type for Si-rich compositions, the $Gd_5Si_2Ge_2$ type for intermediate range of concentrations, and the Sm_5Ge_4 type for Ge-rich alloys. The magnetic properties of the $Sm_5Si_xGe_{4-x}$ compounds can be well described by considering the temperature-independent Van Vleck term due to a small energy separation between the ground state and the first excited state of Sm^{3+} ions. Compared with other light lanthanide $R_5Si_xGe_{4-x}$, magnetic ordering temperatures of $Sm_5Si_xGe_{4-x}$ compounds are much higher than expected from the de Gennes scaling. The change in the magnetic behaviors with the substitution of Ge by Si is also similar to that observed in the $Gd_5Si_xGe_{4-x}$ system. The external magnetic fields up to 10 T have no effect on the magnetism of the $Sm_5Si_xGe_{4-x}$ alloys.

DOI: 10.1103/PhysRevB.76.014415 PACS number(s): 75.20.En, 75.30.−m, 61.66.Dk

INTRODUCTION

The R_5Si_4 and R_5Ge_4 compounds were discovered by Smith *et al.*, who reported an orthorhombic Sm_5Ge_4-type structure for the germanides with R=Nd, Sm, Gd, Tb, Er, and Y and for the silicides with R=Y, Tb-Er.[1] The crystal structure of Sm_5Ge_4 (space group symmetry *Pnma*) was described by three layers of atoms, which are the layer G (only Ge atoms), the layer S (only Sm atoms), and the layer C (combination of Sm and Ge atoms), stacked along the *b* axis in a (GSCSG) sequence.[2] Later, they found that the orthorhombic 5:4 phase is stable for all of the lanthanide germanides R_5Ge_4 except for R=Pm, Eu, and Yb, but for silicides there are two different crystal structures depending on the rare earth element: the Zr_5Si_4-type tetragonal structure for R=La-Nd, and the Sm_5Ge_4-type orthorhombic structure for R=Y, Sm, Gd-Er except for the monoclinically distorted orthorhombic structure of Lu_5Si_4.[3] According to Holtzberg *et al.*,[4] the silicides have relatively high ferromagnetic (FM) ordering temperatures (T_C), i.e., the respective T_C's are 336, 225, 140, 76, and 25 K for R=Gd, Tb, Dy, Ho, and Er, but the germanides are antiferromagnetic (AFM) with the much lower Néel temperatures (T_N) of 47, 30, 40, 21, and 7 K, respectively. Replacing a small amount of Ge with Si in Gd_5Ge_4 induces ferromagnetism at low temperatures in the $Gd_5Si_xGe_{4-x}$ solid solution.[4]

Since the discovery of the giant magnetocaloric effect (GMCE) in $Gd_5Si_2Ge_2$,[5,6] the $R_5Si_xGe_{4-x}$ systems (R=rare earth element) have been broadly studied to uncover the mechanism of their extraordinary magnetoresponsiveness including the giant magnetoresistance and colossal magnetostriction as well as GMCE.[6–8] The phase relationships and crystallography in the $Gd_5Si_xGe_{4-x}$ system were reported by Pecharsky and Gschneidner[9] who identified three structurally distinct phase regions: Gd_5Si_4-type orthorhombic ($2 < x \leqslant 4$), Sm_5Ge_4-type orthorhombic ($0 < x \leqslant 0.8$), and $Gd_5Si_2Ge_2$ type, which is a monoclinically distorted derivative of these two closely related orthorhombic structures ($0.96 \leqslant x \leqslant 2$). Subsequent studies showed that these three solid solution alloys exhibit quite different magnetic behaviors.[8,10]

In contrast to the crystallographic description reported by Smith *et al.*,[3] the $R_5Si_xGe_{4-x}$ systems can be better described as formed by pseudo-two-dimensional, ~7 Å thick slabs that are arranged differently in terms of bonding between the slabs rather than stacking of monolayers.[11,12] All of the slabs, one-half of the slabs, or none of the slabs are interconnected via short T_2 dimers (T=Si and/or Ge) for the Gd_5Si_4-type, the $Gd_5Si_2Ge_2$-type, and the Sm_5Ge_4-type structures, respectively, e.g., see Fig. 1 in Refs. 8 and 13. The interesting physical properties of $Gd_5Si_xGe_{4-x}$ are strongly correlated with the magnetostructural transitions that are characterized by reversible breaking and reforming of the interslab T_2 bonds, which can be controlled by chemical composition, magnetic field, temperature, and pressure. While the interslab bonding differences are preserved in the paramagnetic or antiferromagnetic states depending on the crystal structure type, all of the slabs are always interconnected via the T_2 dimers in the ferromagnetic state, see Fig. 2 in Ref. 8.

Until now, the crystallography and phase relationships have been investigated for more than one-half of the possible $R_5Si_xGe_{4-x}$ pseudobinary systems [R=La,[14] Pr,[15] Nd,[14,16] Gd,[17] Tb,[18] Dy,[14] Er,[19] Yb,[20] Lu,[14] and Y (Ref. 21)]. Still, there are other $R_5Si_xGe_{4-x}$ systems (R=Ce, Sm, Eu, Ho, and Tm) that have not been studied in detail. The 5:4 phases (R_5Si_4 or R_5Ge_4) have not been reported for R=Pm since it is radioactive with the longest half-life of 14 years, and they do not form for R=Eu. The latter has been experimentally verified by us: two alloys prepared as described in the next section at Eu_5Si_4 and Eu_5Ge_4 stoichiometries were clearly two-phase materials, each containing Eu_5Si_3 and EuSi, and Eu_5Ge_3 and EuGe, respectively. For other rare earth metals [R=Ce,[3,22–24] Sm,[1–3] Ho,[3,25,26] and Tm (Refs. 3 and 27)], only the binary silicides and germanides have been reported

TABLE I. Room temperature crystallographic data of $Sm_5Si_xGe_{4-x}$ alloys.

Composition	Structure type	Unit cell dimensions			Distance	Reference
		a, Å	b, Å	c, Å	$d_{T3\text{-}T3}$, Å	
Sm_5Si_4	Gd_5Si_4	7.5738(7)	14.890(1)	7.8156(7)	2.745(2)	This work
Sm_5Si_4	Sm_5Ge_4	7.57	14.88	7.78		3
Sm_5Si_3Ge	Gd_5Si_4	7.5858(6)	14.911(1)	7.8440(6)	2.722(2)	This work
$Sm_5Si_2Ge_2$[a]	$Gd_5Si_2Ge_2$	7.6716(7)	14.945(2)	7.8543(8)	3.821(4)[b]	This work
					2.831(3)[b]	
Sm_5SiGe_3	Sm_5Ge_4	7.7492(5)	14.927(1)	7.8414(6)	3.733(2)	This work
Sm_5Ge_4	Sm_5Ge_4	7.7726(6)	14.947(1)	7.8611(6)	3.754(3)	This work
Sm_5Ge_4	Sm_5Ge_4	7.75	14.94	7.84	3.71(2)	2

[a]γ is 93.344(5)° in the monoclinic structure (space group $P112_1/a$).
[b]There are two kinds of T3-T3 distances in the monoclinic structure; long T3a-T3a and short T3b-T3b distances.

with the exception of the ternary $Ho_5Si_2Ge_2$ compound.[28] Here, we report on the phase relationships, the crystal structures, and the magnetic and thermodynamic properties of both binary and several pseudobinary alloys in the $Sm_5Si_xGe_{4-x}$ system.

EXPERIMENTAL DETAILS

A total of five alloys in the $Sm_5Si_xGe_{4-x}$ system with x varying from 0 to 4 were synthesized by induction melting at ~2070 K for 10 min in sealed Ta crucibles. Prior to induction melting, stoichiometric mixtures of the pure components (Sm, Si, and Ge) were loaded into Ta crucibles, and then the crucibles were sealed under a pure helium atmosphere by arc welding in order to avoid the loss of samarium due to its low boiling temperatures (~2070 K). The Sm metal was prepared by the Materials Preparation Center of the Ames Laboratory[29] and it was 99.5 at. % (99.94 wt. %) pure with major impurities in ppm atomic as follows: F, 1040; Ca, 900; O, 864; C, 125; Cl, 110; Mg, 77; N, 32; Zn, 30; Fe, 27; and Yb, 20. The silicon and germanium, which were purchased from a commercial vendor, were 99.999 wt. % pure. The errors in the compositions due to high vapor pressure of Sm at 2070 K (estimated using the following assumptions: the empty volume of the crucible was ~1.6 cm^3, the sample volume was ~1 cm^3, the vaporized Sm follows ideal gas behavior) were less than 0.2 wt. % (0.04 at. %). The partial vapor pressure of Sm at 2070 K was calculated using data of Ref. 30. Thus, the alloy compositions were accepted in the as-weighed condition. All alloys were investigated in the as-cast condition without additional heat treatment.

The room temperature x-ray powder diffraction was utilized to characterize the crystal structures and phase compositions of the $Sm_5Si_xGe_{4-x}$ alloys. The room temperature x-ray powder diffraction studies were performed on an automated Scintag powder diffractometer using Cu K_α radiation. The crystal structures were refined by using full profile Rietveld refinement technique.[31] Moreover, *in-situ* x-ray powder diffraction measurements of $Sm_5Si_2Ge_2$ were carried out as a function of temperature between 8 and 300 K both on cooling and on heating in a zero magnetic field on a Rigaku TTRAX rotating anode powder diffractometer employing Mo K_α radiation. The sample preparation, instrument setup, and the refinement method employed to process the *in-situ* x-ray powder diffraction data were the same as in Refs. 32–34. The profile residuals were between 7% and 9%, and the derived Bragg residuals were between 3% and 5%.

Magnetic measurements were performed on a SQUID magnetometer (model MPMS XL). The magnetization was measured as a function of temperature from 1.8 to 300 K in 0.05 T, 0.5 T, and 5 T dc magnetic fields. Isothermal magnetization data were collected only around the magnetic ordering temperatures of the alloys and at 1.8 K in dc magnetic fields varying from 0 to 7 T with 0.2 T steps. The heat capacity of the $Sm_5Si_xGe_{4-x}$ alloys was measured using an adiabatic heat-pulse calorimeter[35] from ~3.5 K to 350 K in dc magnetic fields ranging from 0 to 10 T.

RESULTS AND DISCUSSION

Phase relationships and crystallography

As mentioned above, the crystal structure in the paramagnetic (PM) state in the $R_5Si_xGe_{4-x}$ systems is a critical parameter that usually defines physical properties of individual alloys, especially their magnetism. When nonbonded slabs are present in the PM state, these generally become interconnected via short T_2 dimers at or below the ferromagnetic ordering temperature that may occur as first-order magnetic-structural phase transformations.[8] The magnetic phase transitions, if any, are normally second- order when all slabs are connected in the PM state.

The room temperature x-ray powder diffraction measurements were performed for all five alloys in the $Sm_5Si_xGe_{4-x}$ systems in order to investigate their crystallography and phase purity in the PM state. The room temperature crystallographic data including the structure type and lattice parameters are given in Table I and the coordinates of atoms in Table II. Figures 1 and 2 show the observed and calculated powder diffraction patterns of the five alloys. $Sm_5Si_2Ge_2$ and Sm_5Ge_4 are nearly single phase materials (within the sensitivity of the x-ray powder diffraction technique, which given

TABLE II. Atomic coordinates and T-site occupancies of $Sm_5Si_xGe_{4-x}$ compounds.

Compound	Atom/site	x/a	y/b	z/c	g (%)[a]
Sm_5Si_4	Sm1 in 4(c)	0.3574(9)	1/4	0.0104(6)	
	Sm2 in 8(d)	0.0311(5)	0.0972(2)	0.1750(6)	
	Sm3 in 8(d)	0.3151(4)	0.8766(2)	0.1866(5)	
	Si1 in 4(c)	0.225(1)	1/4	0.342(3)	100
	Si2 in 4(c)	0.001(3)	1/4	0.926(3)	100
	Si3 in 8(d)	0.146(3)	0.947(1)	0.479(3)	100
Sm_5Si_3Ge	Sm1 in 4(c)	0.3507(8)	1/4	0.0096(7)	
	Sm2 in 8(d)	0.0258(5)	0.0967(2)	0.1792(5)	
	Sm3 in 8(d)	0.3161(4)	0.8781(2)	0.1828(5)	
	T1 in 4(c)	0.223(2)	1/4	0.339(2)	41.2[b]
	T2 in 4(c)	0.997(3)	1/4	0.925(3)	82[b]
	T3 in 8(d)	0.187(2)	0.962(1)	0.484(2)	66.4[b]
$Sm_5Si_2Ge_2$	Sm1 in 4(e)	0.3211(1)	0.2544(6)	−0.0066(9)	
	Sm2a in 4(e)	−0.0117(9)	0.0986(5)	0.1729(1)	
	Sm2b in 4(e)	0.0116(1)	0.4009(5)	0.1935(1)	
	Sm3a in 4(e)	0.3645(1)	0.8850(5)	0.1630(1)	
	Sm3b in 4(e)	0.3320(1)	0.6221(5)	0.1788(1)	
	T1 in 4(e)	0.198(3)	0.247(2)	0.366(3)	50[c]
	T2 in 4(e)	0.943(3)	0.256(2)	0.908(2)	50[c]
	T3a in 4(e)	0.228(3)	0.956(1)	0.479(3)	50[c]
	T3b in 4(e)	0.150(3)	0.558(1)	0.475(3)	50[c]
Sm_5SiGe_3	Sm1 in 4(c)	0.2883(7)	1/4	0.0002(7)	
	Sm2 in 8(d)	−0.0215(4)	0.0998(2)	0.1817(5)	
	Sm3 in 8(d)	0.3803(4)	0.8841(2)	0.1633(4)	
	T1 in 4(c)	0.173(1)	1/4	0.370(2)	25[c]
	T2 in 4(c)	0.915(2)	1/4	0.898(1)	25[c]
	T3 in 8(d)	0.221(1)	0.953(4)	0.469(1)	25[c]
Sm_5Ge_4	Sm1 in 4(c)	0.2909(7)	1/4	0.0011(6)	
	Sm2 in 8(d)	−0.0187(4)	0.1000(2)	0.1862(5)	
	Sm3 in 8(d)	0.3808(4)	0.8853(2)	0.1647(4)	
	Ge1 in 4(c)	0.178(1)	1/4	0.362(1)	100
	Ge2 in 4(c)	0.929(2)	1/4	0.905(1)	100
	Ge3 in 8(d)	0.222(1)	0.952(1)	0.474(1)	100

[a]Occupancy by the Si atoms with the remainder occupied by the Ge atoms except for Sm_5Ge_4, where the value is for the site occupancies by the Ge atoms.

[b]Occupancies of the T sites have been refined with the only imposed constraint that each site has 100% overall occupancy.

[c]The actual occupancies were not refined—they were assigned based on the as-prepared stoichiometry assuming completely random distribution of the Si and Ge atoms.

the quality of data may be estimated at ~98 vol. % pure or better), but there were small amounts of the 5:3 impurity phases in Sm_5Si_4, Sm_5Si_3Ge, and Sm_5SiGe_3; the concentration levels were 5.7, 7.6, and 4.6 vol. %, respectively, as determined from the Rietveld refinements. The lattice parameters as a function of Si content, x(Si), are shown in Fig. 3. In the $R_5Si_xGe_{4-x}$ systems, all lattice parameters generally decrease with the replacement of Ge by Si because of the smaller atomic radius of Si. In the $Sm_5Si_xGe_{4-x}$ system, there are small discontinuous changes in the b and c lattice parameters coinciding with the structural changes from the Sm_5Ge_4-type to the $Gd_5Si_2Ge_2$-type and the Gd_5Si_4-type structures, but the greatest change occurs in the lattice parameter a. This is similar to the $Gd_5Si_xGe_{4-x}$ system, which exhibits the same phase sequence when Si is substituted for Ge.

Lattice parameters in the known binary 5:4 rare earth silicides, germanides, and ternary $R_5Si_xGe_{4-x}$ compounds with the same crystal structure (except for Yb_5Ge_4, which unlike all other germanides has the Gd_5Si_4-type structure) are plotted as a function of the atomic number of the rare earth element in Fig. 4. Even though the Sm ions in some compounds may have divalent, or trivalent, or mixed valence state, in the $Sm_5Si_xGe_{4-x}$ system the Sm ion appears to be

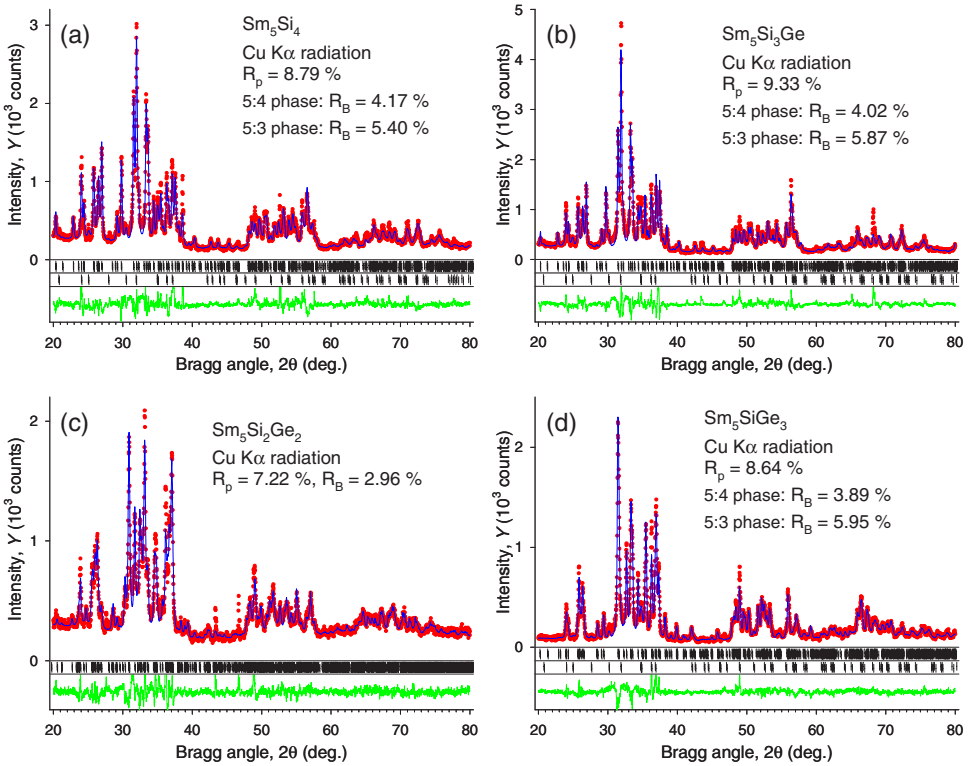

FIG. 1. (Color online) The observed (dots) and calculated (lines drawn through the data points) powder diffraction patterns of Sm_5Si_4, Sm_5Si_3Ge, $Sm_5Si_2Ge_2$, and Sm_5SiGe_3 after the completion of Rietveld refinements. The upper sets of vertical bars located just below the plots of the observed and calculated intensities indicate the calculated positions of the Bragg peaks of the majority 5:4 phase, while the lower sets of bars correspond to the calculated positions of the Bragg peaks of the 5:3 impurity. The differences, $Y_{obs}-Y_{calc}$, are shown at the bottom of the plot. Several strong Bragg peaks observed between 40° and 50° that do not match the calculated pattern in (c) are experimental artifacts that result from spotty Debye rings.

trivalent because their lattice parameters follow the normal lanthanide contraction with the increasing atomic number.

Magnetic properties

The isofield magnetization as a function of temperature and the isothermal magnetization as a function of magnetic field were measured to characterize the type of magnetic ordering and to derive the magnetic ordering transition temperatures, the effective magnetic moments, and the ordered magnetic moments.

The free trivalent Sm ion has five $4f$ electrons ($L=5$ and $S=5/2$) and in a solid the ^6H levels are split by the spin-orbit interaction into the ground state $^6H_{5/2}$, the excited states $^6H_{7/2}, ^6H_{9/2}, \ldots, ^6H_{15/2}$ J multiplets.[36] The consecutive multiplet energy interval between the ground state ($^6H_{5/2}$) and the first excited state ($^6H_{7/2}$) is only ~930 cm^{-1}, so that the Van Vleck theory includes a second term, which is especially important for Sm (and Eu) ions but is negligible for heavy lanthanides.[37] Therefore, the Van Vleck term plays a major role in modeling the magnetic susceptibility of Sm com-

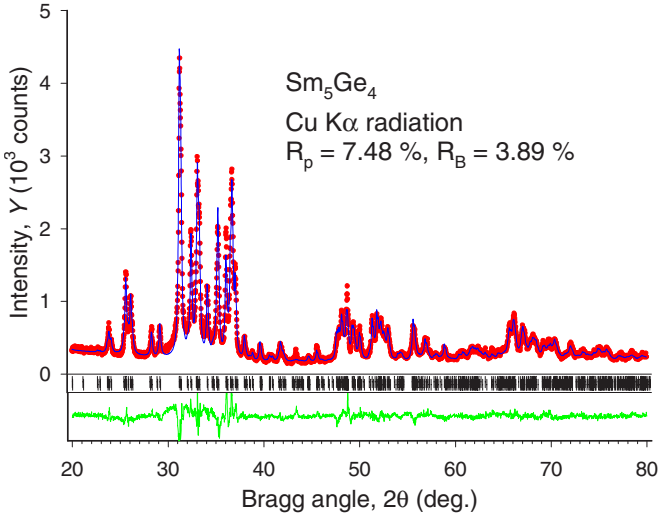

FIG. 2. (Color online) The observed (dots) and calculated (lines drawn through the data points) powder diffraction pattern of Sm_5Ge_4 after the completion of Rietveld refinements. The calculated positions of the Bragg peaks are shown as vertical bars just below the plots of the observed and calculated intensities. The differences, $Y_{obs}-Y_{calc}$, are shown at the bottom of the plot.

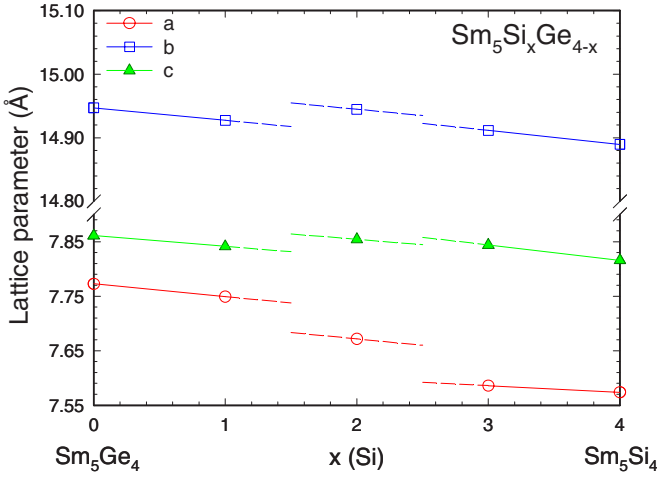

FIG. 3. (Color online) Lattice parameters as a function of x in the $Sm_5Si_xGe_{4-x}$ system. Sm_5Ge_4 and Sm_5SiGe_3 have the Sm_5Ge_4-type structure; $Sm_5Si_2Ge_2$ has the $Gd_5Si_2Ge_2$-type structure; and Sm_5Si_3Ge and Sm_5Si_4 have the Gd_5Si_4-type structure.

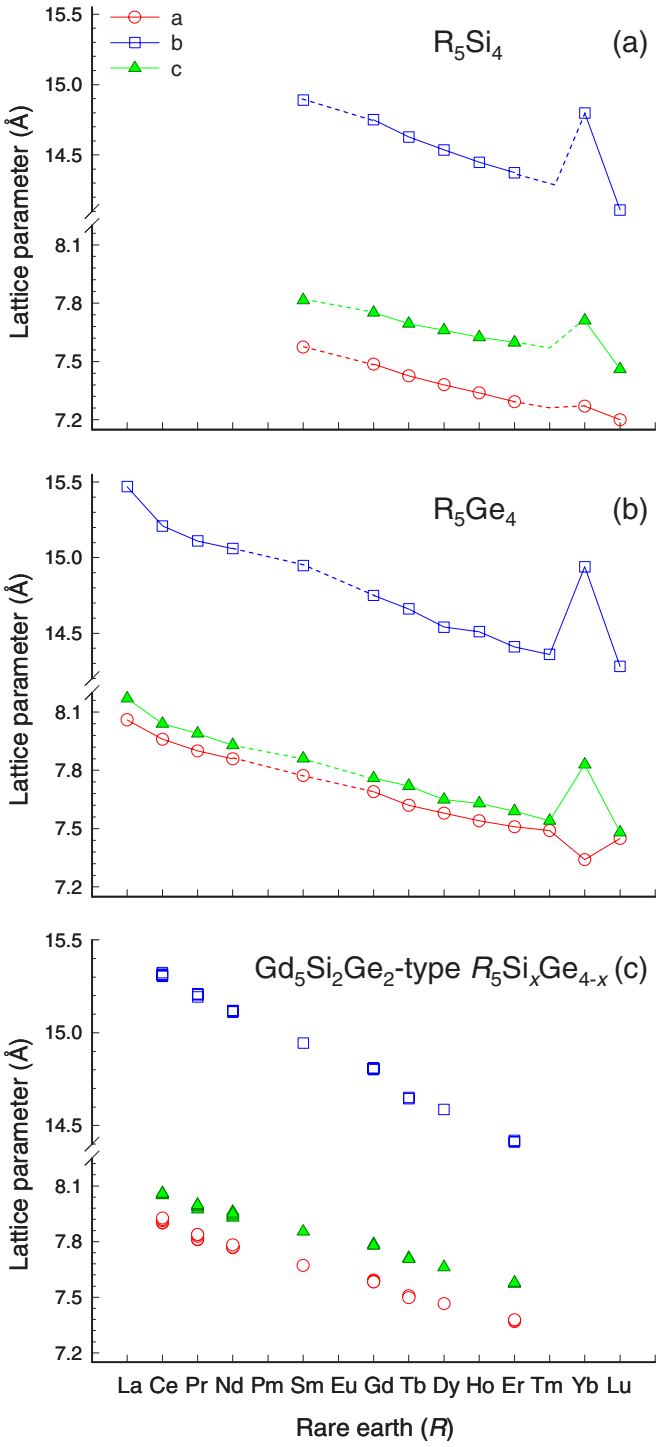

FIG. 4. (Color online) The unit cell parameters of the isostructural R_5Si_4 (Gd_5Si_4-type structure), R_5Ge_4 (Sm_5Ge_4-type structure except for Yb_5Ge_4, which has the Gd_5Si_4-type structure), and $R_5Si_xGe_{4-x}$ ($Gd_5Si_2Ge_2$-type structure) plotted as a function of the atomic number.

pounds because of the varying population of the excited levels and second-order Zeeman splitting. Normally, the Curie part of the susceptibility in Sm compounds is considerably smaller compared to other lanthanide compounds because the g_J (Landé splitting factor) of the ground state ($J=5/2$) is only 2/7. Thus, in principle, in the calculation of the susceptibility of the metallic compounds containing Sm^{3+} ions, there are various factors to be considered: the crystalline electric field (CEF) splitting of a ground state and the low level excited states of the J multiplet, Ruderman-Kittel-Kasuya-Yosida (RKKY) interaction, the Van Vleck transition between different J multiplets, which are caused both by the applied magnetic field and by the exchange fields, the effect of conduction-electron polarization due to $4f$ moments, and the thermal population of higher-lying J multiplets. With the consideration of these factors, the susceptibility calculation of metallic tripositive Sm compounds has been reported by several groups.[37–41] Stewart[40] reported that when only the conduction electron polarization, interionic Heisenberg exchange interaction, and the thermally populated admixture of the $^6H_{7/2}$ into the $^6H_{5/2}$ state are taken into account, the susceptibility $\chi(T)$ can be well described by a simple form

$$\chi(T) = \chi_0 + C/(T - \theta_p) \quad (1)$$

without considering the CEF splitting. Here, χ_0 is the temperature-independent Van Vleck term due to the admixture of the first excited angular momentum state ($J=7/2$) to the unperturbed ground state ($J=5/2$) when either a magnetic field is applied or a temperature is high enough to allow thermal population. In the Curie-Weiss term, $C/(T-\theta_p)$, arising from the ground state ($J=5/2$), C is the Curie constant, T is the absolute temperature, and θ_p is the Weiss temperature.

The magnetization of $Sm_5Si_xGe_{4-x}$ alloys is shown in Figs. 5 and 6. Irrespective of the dc magnetic fields, including 0.5 T and 5 T data, the magnetizations of Sm_5Si_4, Sm_5Si_3Ge, and $Sm_5Si_2Ge_2$ shown in Fig. 5 exhibit a broad maximum around the magnetic ordering temperature, and then decrease with the decreasing temperature showing nearly constant values below ~50 K. This behavior mimics ferrimagnetic arrangements of spins, but different temperature dependencies of spin and orbital magnetic moments arising from ferromagnetically aligned Sm^{3+} ions may also induce such behavior.[42–45] On the other hand, both Sm_5SiGe_3 and Sm_5Ge_4 seem to order antiferromagnetically around 90 K, but there are upturns in their magnetizations below ~50 K, which are uncommon for a conventional AFM, see Fig. 6.

The isothermal magnetization data, measured just below the magnetic ordering temperatures that are shown in Figs. 7(b), 7(d), and 7(f), confirm that Sm_5Si_4, Sm_5Si_3Ge, and $Sm_5Si_2Ge_2$ order ferromagnetically with low saturation magnetization (M_S) values, but with a substantial coercivity (H_C), and hysteresis. At 1.8 K [Figs. 7(a), 7(c), and 7(e)], none of the compounds approach saturation and all of them exhibit narrower hysteresis. On the other hand, the isothermal magnetizations of the Ge-rich compounds measured at 80 K and seen in Figs. 7(h) and 7(j) are nearly linear functions of the magnetic field between 0 and 7 T; this behavior changes little at 1.8 K. The magnetic behavior in the $Sm_5Si_xGe_{4-x}$ system is consistent with other $R_5Si_xGe_{4-x}$ systems where the ferromagnetic or ferromagneticlike ground state is found in Si-rich alloys changing over to the AFM state for Ge-rich alloys. The dc magnetic susceptibility of $Sm_5Si_2Ge_2$ in the field-cooled (FC) cooling regime does not

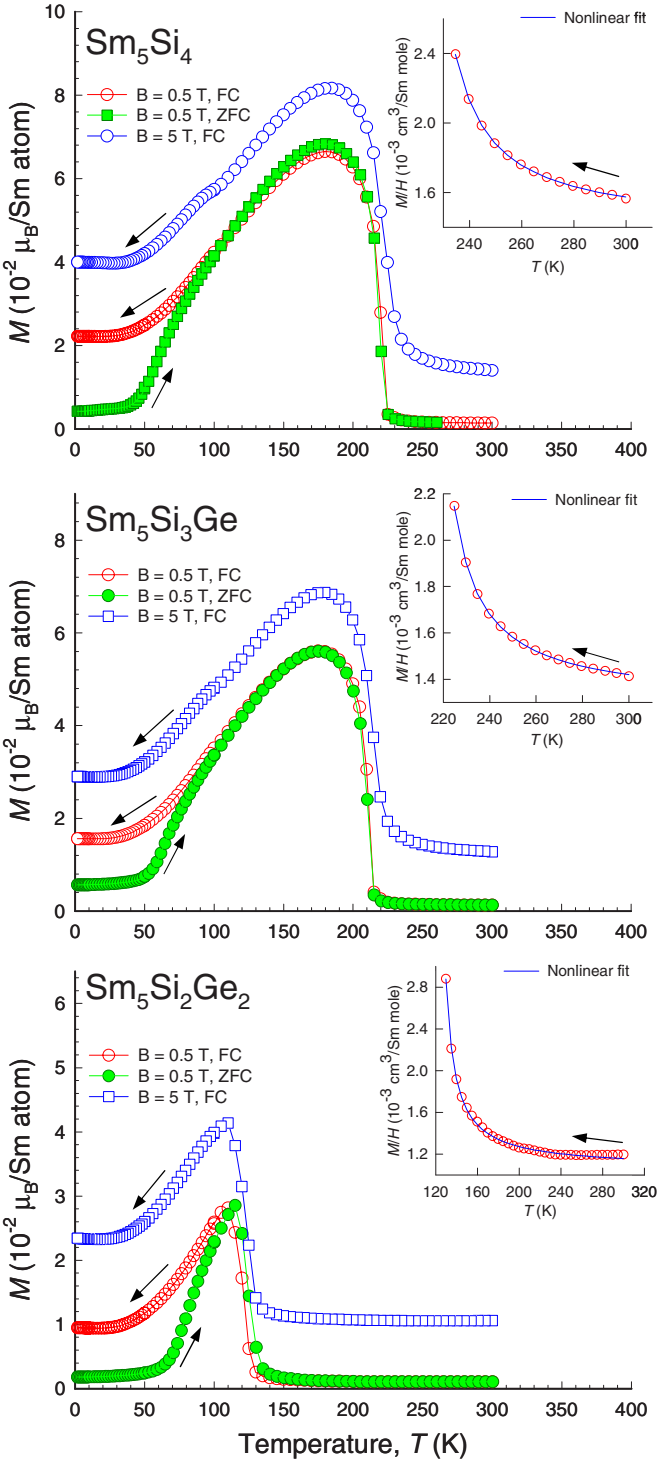

FIG. 5. (Color online) The magnetization of Sm_5Si_4, Sm_5Si_3Ge, and $Sm_5Si_2Ge_2$ measured in dc magnetic fields of 0.5 T and 5 T. Insets show the nonlinear fits of the magnetic susceptibilities measured in 0.5 T fields in the paramagnetic regime using Eq. (1).

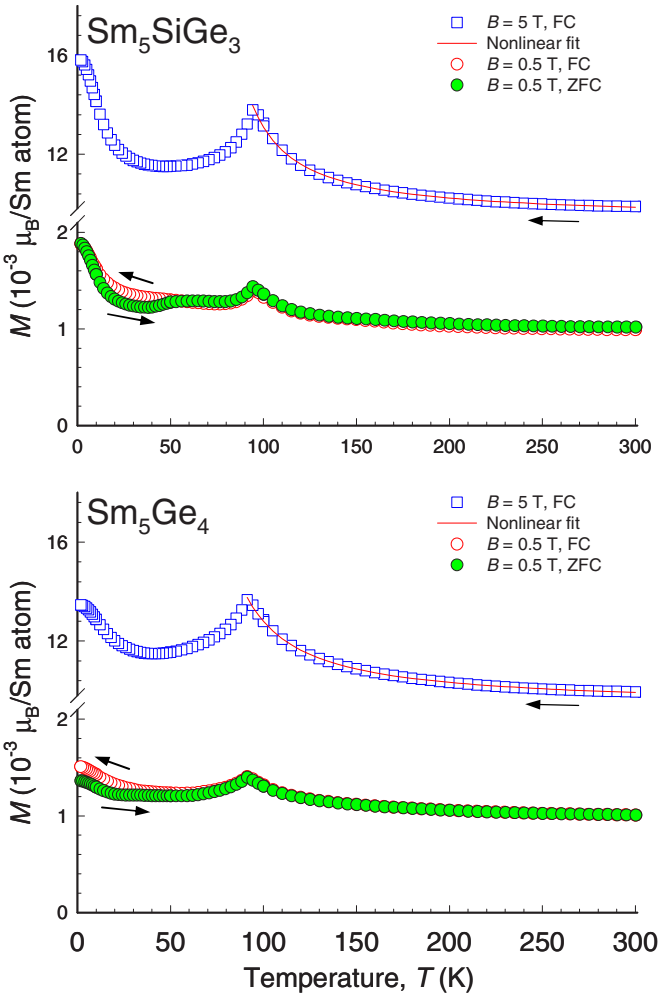

FIG. 6. (Color online) The magnetization of Sm_5SiGe_3 and Sm_5Ge_4 measured in dc magnetic fields of 0.5 T and 5 T. Lines drawn through the data points are nonlinear fits of the magnetic susceptibilities measured in 5 T fields using Eq. (1).

match that in the zero-field-cooled (ZFC) heating regime around the magnetic ordering temperature exhibiting a Curie temperature difference of ~10 K between the heating and cooling branches (Fig. 5), which is consistent with a first-order magnetic phase transition. There is no measurable hysteresis of T_C in Sm_5Si_4 and Sm_5Si_3Ge nor is there a hysteretic behavior around T_N in Sm_5SiGe_3 and Sm_5Ge_4, which is consistent with second-order magnetic phase transitions. Moreover, the Sm_5Ge_4-type compounds show no features consistent with magnetostructural changes despite the absence of the interslab T_2 bonds in the PM state.

As mentioned above, the dc magnetic susceptibilities of these compounds in the paramagnetic state cannot be described by a simple Curie-Weiss law because of the nonlinearity of $1/\chi$ above the magnetic ordering temperature, but they can be well fitted by the modified Curie-Weiss law [Eq. (1)]. Especially, in the case of tripositive Sm compounds,

$$\chi(T) = \chi_0 + C/(T-\theta_p) = \left(\frac{N_A}{k_B}\right)\left(\alpha_J \mu_B^2 + \frac{\mu_{\text{eff}}^2}{3(T-\theta_p)}\right) \quad (2)$$

can be derived, where N_A is Avogadro's number, k_B is Boltzmann constant, μ_B is the Bohr magneton, μ_{eff} is the effective magnetic moment in Bohr magnetons, and

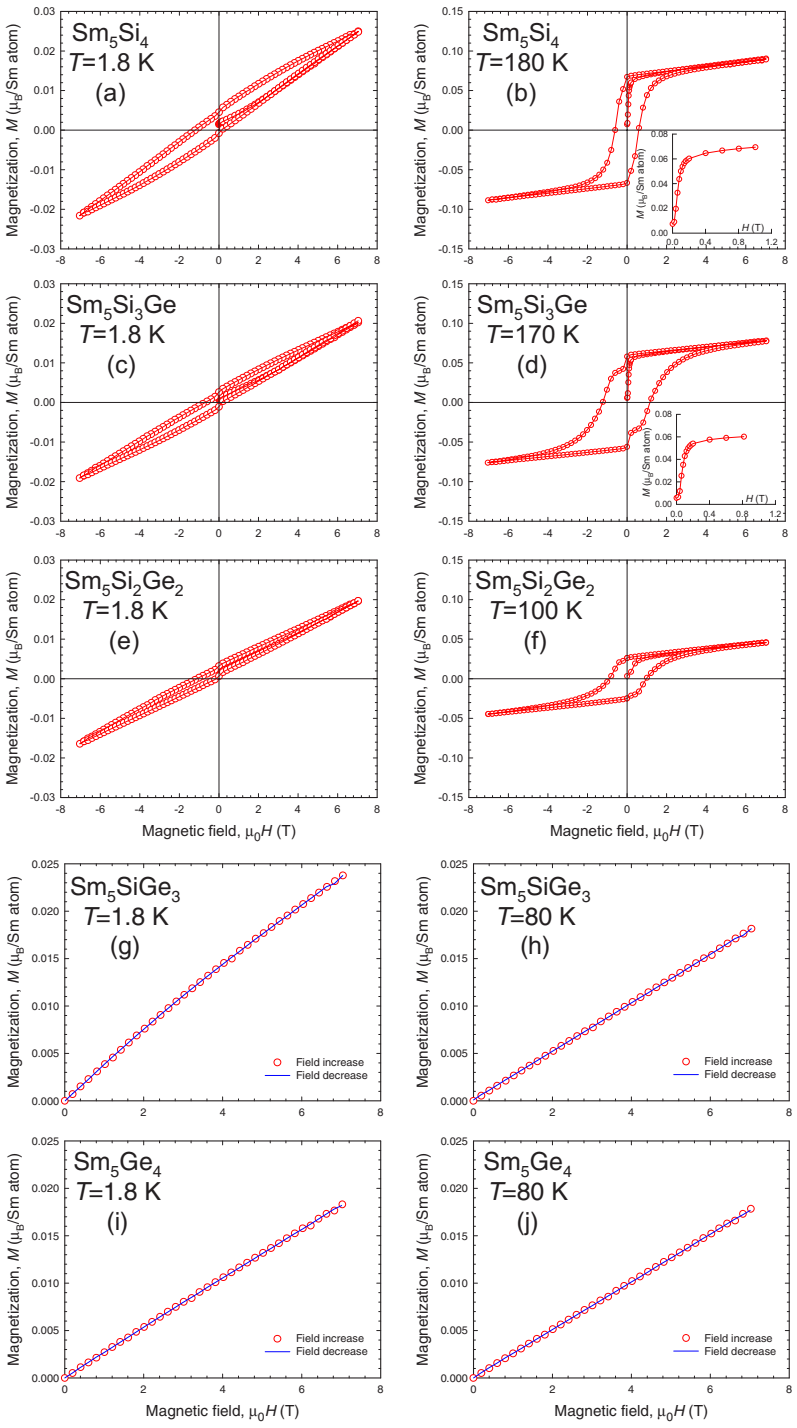

FIG. 7. (Color online) The magnetization as a function of magnetic field measured at 1.8 K and a few Kelvin below the magnetic phase transition temperatures for (a) and (b) Sm_5Si_4, (c) and (d) Sm_5Si_3Ge, (e) and (f) $Sm_5Si_2Ge_2$, (g) and (h) Sm_5SiGe_3, (i) and (j) Sm_5Ge_4. Insets in (b) and (d) show initial magnetizations in magnetic fields between 0 and 1 T.

$$\alpha_J = k_B\left(\frac{(J^2-(L-S)^2)[(L+S+1)^2-J^2]}{6J(2J+1)(E_{J-1}-E_J)} + \frac{[(J+1)^2-(L-S)^2][(L+S+1)^2-(J+1)^2]}{6(J+1)(2J+1)(E_{J+1}-E_J)}\right) \quad (3)$$

is $20/7\Delta$, where Δ is the energy separation (expressed in units of K) between $J=7/2$ and $J=5/2$ states.[46] Thus, the best fitting parameters Δ, μ_{eff}, and θ_p, extracted from the nonlinear least square fits of the dc magnetic susceptibilities are listed in Table III along with other basic magnetic quantities. The root mean square (rms) errors for nonlinear fits were less than 0.7% except for $Sm_5Si_2Ge_2$ where they were 3%. The Van Vleck terms χ_0 in the $Sm_5Si_xGe_{4-x}$ system range between 1.04×10^{-3} cm^3/Sm mole for Sm_5Ge_4 and 1.38×10^{-3} cm^3/Sm mole for Sm_5Si_4, which compares well with the value of 1.18×10^{-3} cm^3/mole obtained in Ref. 40 for the rhombohedral Sm metal.

Even though both Sm_5SiGe_3 and Sm_5Ge_4 are likely to have an AFM ground state, their paramagnetic Curie temperatures, θ_P, are positive (70 and 60 K, respectively), which is one of the most unusual features of all of the other AFM

TABLE III. The magnetic properties of $Sm_5Si_xGe_{4-x}$ compounds.

Composition	T_C (K)[a]	Θ_P (K)	$\mu_{eff}(\mu_B)$	μ at 1.8 K (μ_B)[c]	μ at $\sim T_C$ (μ_B)[d]	χ_0 (10^{-3} cm^3/Sm mole)	Δ (K)[e]
Sm_5Si_4	220	220	0.34	0.025	0.1	1.38	776
Sm_5Si_3Ge	210	212	0.29	0.02	0.08	1.30	824
$Sm_5Si_2Ge_2$	125	120	0.36	0.02	0.05	1.07	1000
Sm_5SiGe_3	90[b]	70	0.31	0.024	0.018	1.04	1030
Sm_5Ge_4	90[b]	60	0.35	0.018	0.018	1.04	1030

[a]T_C or T_N from the C_P measurement.
[b]Néel temperature (T_N).
[c]The magnetic moment per Sm atom in a 7 T magnetic field at $T=1.8$ K.
[d]The magnetic moment per Sm atom in a 7 T magnetic field between 10 and 40 K below the magnetic transition temperature.
[e]Energy separation between $J=7/2$ and $J=5/2$ states.

R_5Ge_4 compounds studied to date (i.e., $\theta_P=94$ K for $R=$Gd, 80 K for Tb, 43 K for Dy, 16 K for Ho, and 10 K for Er).[4] The effective magnetic moments of the $Sm_5Si_xGe_{4-x}$ alloys range between 0.29 and 0.36 μ_B/Sm atom, which is considerably smaller than the theoretical effective magnetic moment of the free Sm^{3+} ion (0.85 μ_B/Sm atom), while Δ ranges between 776 K and 1030 K; all are lower than $\sim$1350 K estimated for free Sm^{3+} ions.[37] The reduced effective magnetic moments in the $Sm_5Si_xGe_{4-x}$ alloys are probably due to the effect of CEF splitting of the Hund's rule ground state because crystal fields can also admix the ground and excited levels and thus affect the magnetic susceptibility. The low Δ values have been reported for other Sm-based compounds.[47,48]

The magnetization values around the Curie temperatures for Sm_5Si_4, Sm_5Si_3Ge, and $Sm_5Si_2Ge_2$ are $\sim$0.091, 0.076, and 0.046 μ_B/Sm atom, respectively, obtained in the maximum field of our apparatus (7 T), which are only $\sim$12.8%, 10.7%, and 6.5% of the theoretical value of the saturation magnetization $M_{sat}=g_JJ\mu_B=0.71\mu_B$/Sm atom. The possible causes for the low saturation magnetization values at high magnetic fields are the magnetic anisotropy, second-order Zeeman effects, and CEF. Interestingly, high coercive fields H_C of $\sim$0.7, 1.4, and 1 T are observed in close proximity of T_C for Sm_5Si_4, Sm_5Si_3Ge, and $Sm_5Si_2Ge_2$, respectively, see Fig. 7. Moreover, the T_C and T_N values for Sm compounds ($T_C=220$ K for Sm_5Si_4 and $T_N=90$ K for Sm_5Ge_4) are much higher than expected from the de Gennes scaling in light lanthanide elements (Ce, Pr, Nd, and Sm).

Heat capacity

The heat capacity (C_P) data of all alloys in the $Sm_5Si_xGe_{4-x}$ system are shown as a function of temperature between $\sim$3.5 K and 350 K in magnetic fields of 0 and 10 T in Figs. 8 and 9. The peak shapes of C_P for Sm_5Si_4, Sm_5Si_3Ge, Sm_5SiGe_3, and Sm_5Ge_4 at either T_C or T_N have the typical lambda shape of a material which exhibits a second-order magnetic transformation, but that for $Sm_5Si_2Ge_2$ is indicative of a broad first-order phase transition at $T_C=125$ K. The magnetic ordering temperatures from C_P data are in good agreement with those from the dc sus-

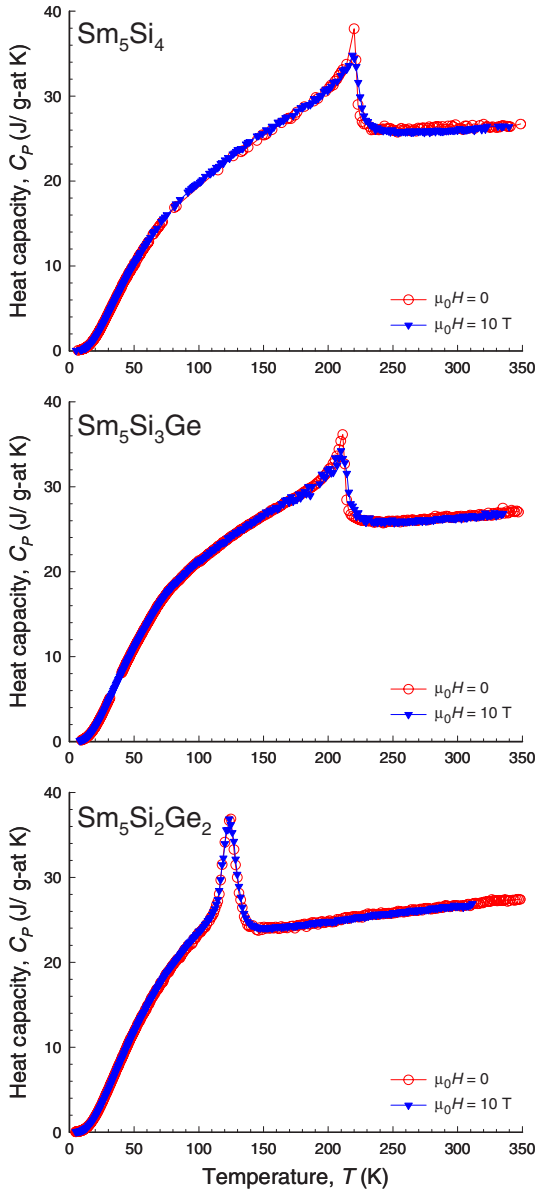

FIG. 8. (Color online) The heat capacities of Sm_5Si_4, Sm_5Si_3Ge, and $Sm_5Si_2Ge_2$ measured in 0 and 10 T magnetic fields measured on heating.

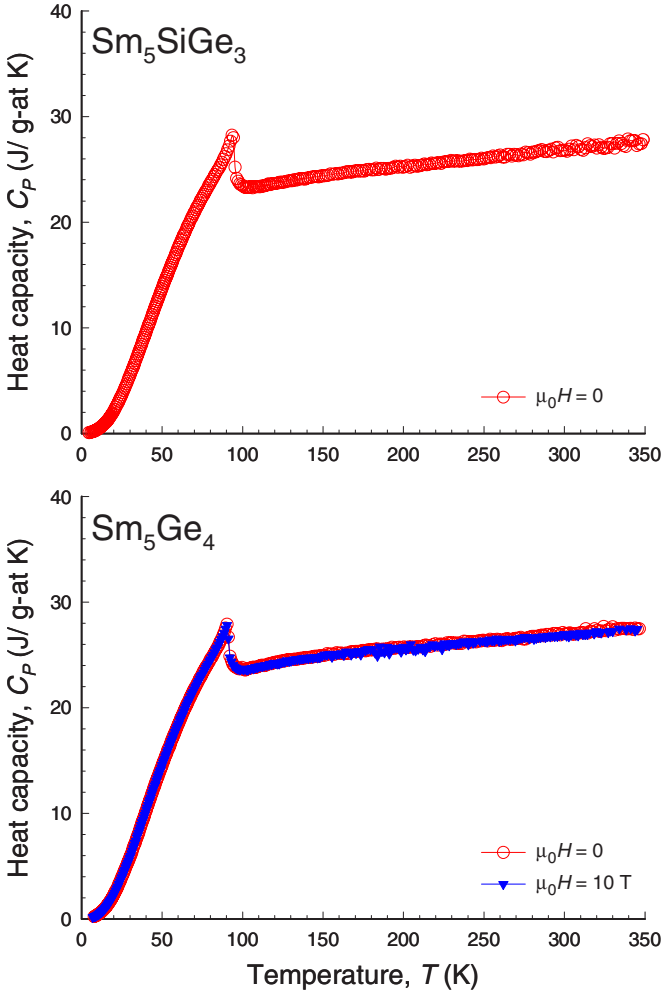

FIG. 9. (Color online) The heat capacities of Sm_5SiGe_3 and Sm_5Ge_4 measured in 0 and 10 T magnetic fields measured on heating.

ceptibilities. Interestingly, the C_P data for 10 T (the highest magnetic field available in our calorimeter) are nearly superimposed on those for zero magnetic field in all the alloys, that is, the external magnetic field has little to no effect on the magnetic entropy. In general, the magnetocaloric effect (MCE) as the isothermal magnetic entropy change, ΔS_{mag}, and the adiabatic temperature change, ΔT_{ad} can be calculated from the C_P data as described by Pecharsky and Gschneidner.[49] Since $\Delta S_{mag}=S(B,T)-S(0,T)=\int_0^T \frac{C(B,T)-C(0,T)}{T} dT$, the MCE in the $Sm_5Si_xGe_{4-x}$ system is expected to be negligibly small because of roughly overlapping C_P data, i.e., $C(B,T)\cong C(0,T)$.

The heat capacities of nonmagnetic analogs R_5Si_4, R_5Ge_4, and $R_5Si_2Ge_2$ for R=La and Lu were used to estimate the electronic and lattice contributions to the heat capacities of magnetic Sm_5Si_4, Sm_5Ge_4, and $Sm_5Si_2Ge_2$, and thus determine the purely magnetic heat capacities of these compounds. The molar magnetic entropies of Sm_5Si_4, Sm_5Ge_4, and $Sm_5Si_2Ge_2$ are plotted in Fig. 10. At ~350 K they reach 71%, 74%, and 71% of the theoretical maximum molar magnetic entropy of the Sm^{3+} ion (J=5/2) of $5R$ ln 6, i.e., $S_{mag}=R\ln(2J+1)$ J/mol K, respectively (where R=8.31 J/mol K

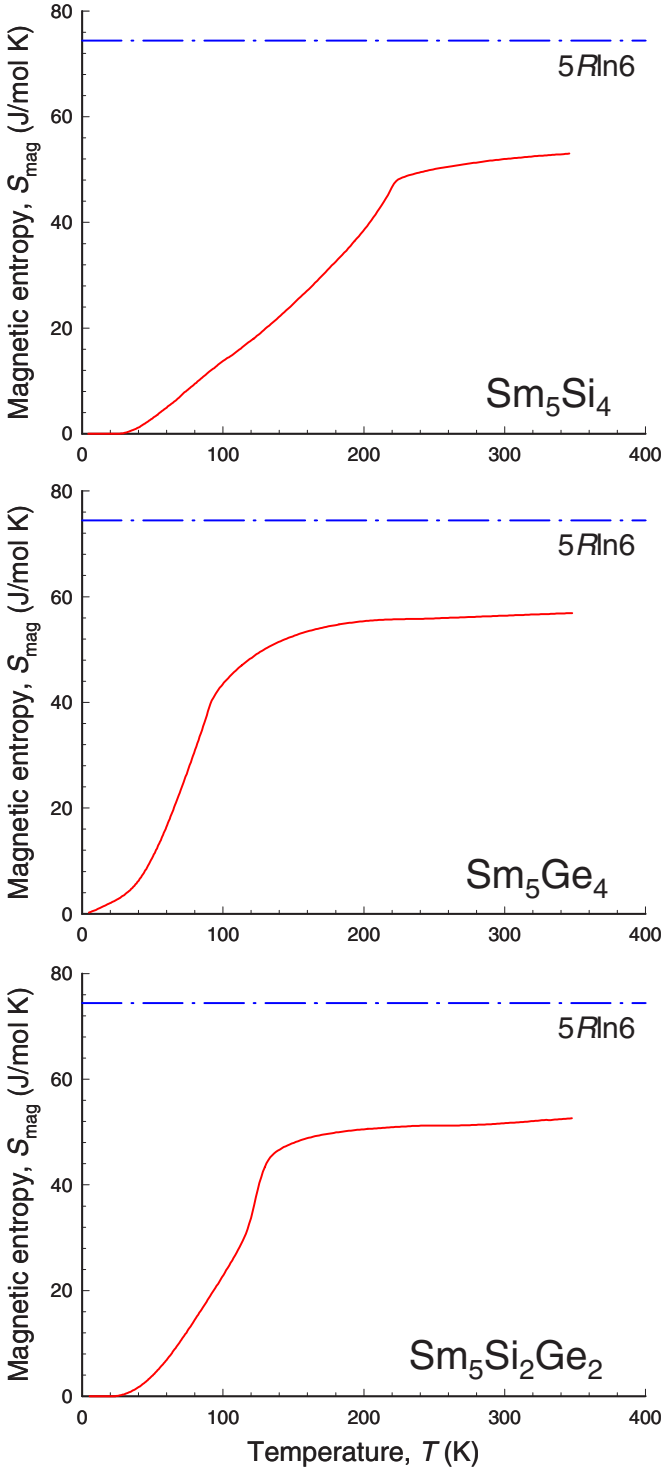

FIG. 10. (Color online) The molar magnetic entropies of Sm_5Si_4, Sm_5Ge_4, and $Sm_5Si_2Ge_2$ in zero magnetic field.

is the molar gas constant). In any case the magnetic entropy should attain its full $R\ln(2J+1)$ value for 1 mole of $4f$ ions at high temperature. With all the rare earths except Gd, the entropy does not reach this maximum value because of CEF splitting. Furthermore, there is a clear indication of a first-order magnetostructural transition in the molar magnetic entropy of $Sm_5Si_2Ge_2$ in Fig. 10 and thus the change of the entropy during the structural transformation (ΔS_{str}) can be

TABLE IV. The Gd_5Si_4-type crystal structure of the low-temperature (LT) $Sm_5Si_2Ge_2$ at 8 K in a zero magnetic field. The space group symmetry is *Pnma*.

	T=8 K, H=0 kOe		
	LT-$Sm_5Si_2Ge_2$, a=7.594(2), b=14.898(3), c=7.846(1) Å		
Atom	x/a	y/b	z/c
Sm1	0.3542(2)	1/4	0.0132(1)
Sm2	0.0229(9)	0.0981(3)	0.1780(1)
Sm3	0.3236(8)	0.8787(4)	0.1741(1)
T1	0.221(3)	1/4	0.349(4)
T2	0.966(4)	1/4	0.930(3)
T3	0.171(3)	0.955(1)	0.484(3)

easily estimated. It is approximately equal to that of $Gd_5Si_2Ge_2$ (ΔS_{str}=1.08 J/g at. K).[50]

Low-temperature crystallography and preliminary phase diagram

Since both the heat capacity and magnetization of $Sm_5Si_2Ge_2$ point to a first-order transformation, likely coupled with a polymorphic transition, we studied the temperature dependence of the crystal structure of this compound. The crystallographic data and coordinates of atoms of low-temperature (LT) $Sm_5Si_2Ge_2$ at 8 K in a zero magnetic field, which has the Gd_5Si_4-type structure, are listed in Table IV. The observed x-ray powder diffraction patterns of $Sm_5Si_2Ge_2$, which were collected in a zero magnetic field during cooling from 300 K to 8 K, are shown in Fig. 11. There are distinguishable differences in the positions and intensities of Bragg peaks between the low-temperature (Gd_5Si_4-type orthorhombic structure) and high-temperature ($Gd_5Si_2Ge_2$-type monoclinic structure) patterns, which indicate that a structural phase transformation begins around ~115 K on cooling. These crystallographic changes are similar to those observed in $Gd_5Si_2Ge_2$ (Ref. 11) and $Tb_5Si_2Ge_2$.[18]

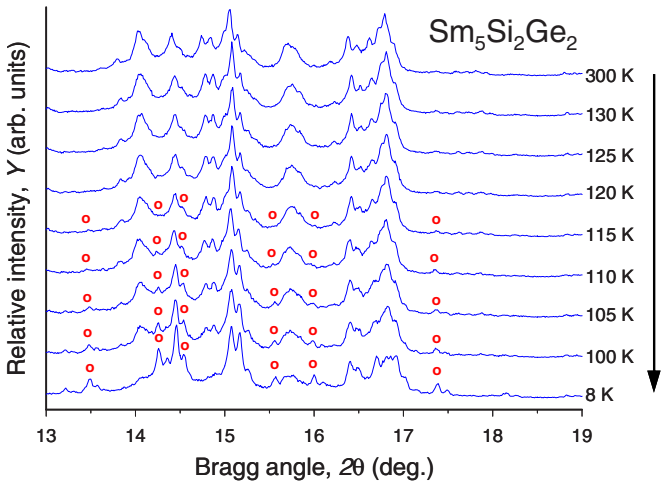

FIG. 11. (Color online) The observed x-ray powder diffraction patterns of $Sm_5Si_2Ge_2$ collected in a zero magnetic field during cooling from 300 K to 8 K. All patterns were collected using Mo K_α radiation. Only the range from 13° to 19° 2θ is shown for clarity. The letter *O* indicates selected characteristic Bragg peaks of the Gd_5Si_4-type orthorhombic phase.

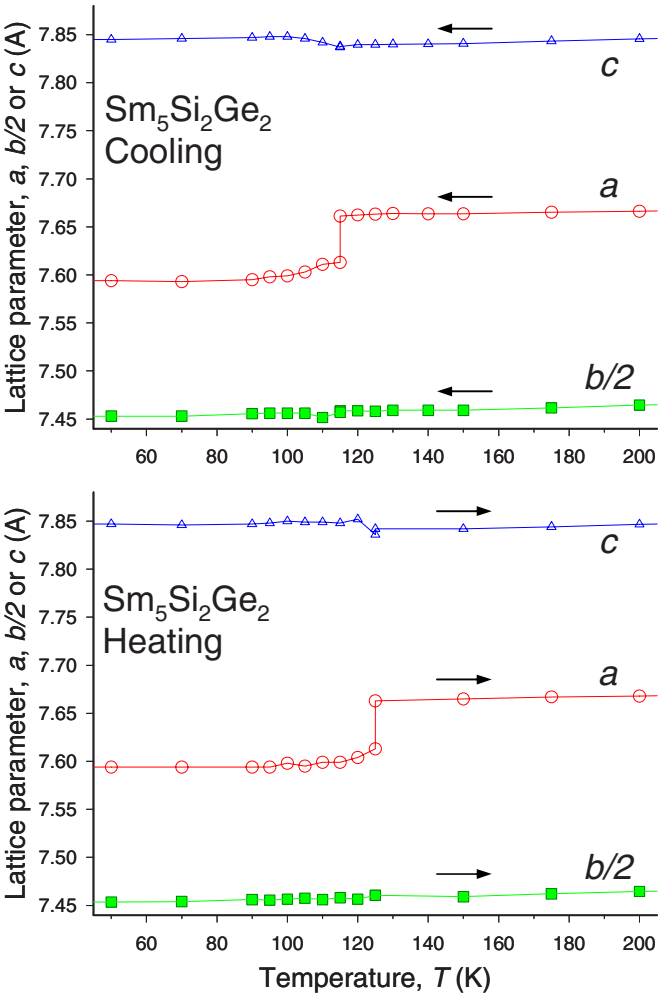

FIG. 12. (Color online) Temperature dependencies of the unit cell dimensions of the major component during cooling of $Sm_5Si_2Ge_2$ (top) and during heating (bottom) in a zero magnetic field. The error bars are smaller than the size of the symbols.

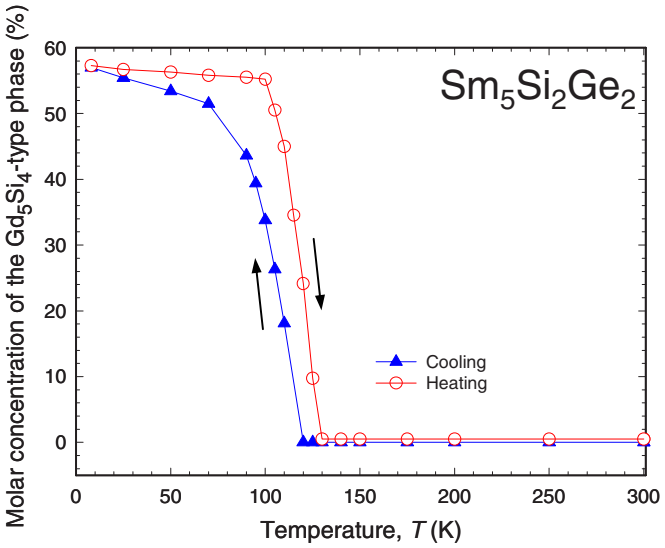

FIG. 13. (Color online) The concentration of the orthorhombic Gd_5Si_4-type phase as a function of temperature determined from Rietveld refinement of the patterns collected during cooling and heating of the $Sm_5Si_2Ge_2$ sample in a zero magnetic field.

The temperature dependencies of the unit cell parameters observed during the temperature-induced structural transformations are illustrated in Fig. 12 for heating and cooling in a zero magnetic field. As the temperature induces the $Gd_5Si_2Ge_2$-type to the Gd_5Si_4-type transformation around 115 K on cooling in the zero magnetic field, the unit cell volume decreases by $\Delta V/V=-0.48\%$ and the lattice parameters change by -0.63%, -0.02%, and $+0.01\%$ along the a, b, and c axes, respectively. Reverse structural transformation is completed around 125 K on heating and the unit cell volume increases by $\Delta V/V=+0.55\%$ and the lattice parameters change by $+0.66\%$, $+0.01\%$, and -0.08% along the a, b, and c axis, respectively.

The temperature dependencies of the molar concentrations of the Gd_5Si_4-type $Sm_5Si_2Ge_2$ phase derived from the Rietveld refinement of the x-ray patterns are shown in Fig. 13. The structural transformation from the Gd_5Si_4 type to the $Gd_5Si_2Ge_2$ type on heating is nearly complete, but the transformation on cooling is incomplete. Even at 8 K, the concentration of the monoclinic $Gd_5Si_2Ge_2$, type phase amounts to $\sim$40%. A similar phenomenon was also reported in *in-situ* x-ray powder diffraction studies of Gd_5Ge_4, with $\sim$6.5% of the high-temperature phase retained at low temperatures, which was explained by existence of microstructure imperfections, such as impurity and defects.[33] The much greater degree of incompleteness of the monoclinic-to-orthorhombic transformation in $Sm_5Si_2Ge_2$ compared to closely related compounds with Gd (Ref. 33) and Tb (Refs. 18 and 51) is consistent with a reduced spin magnetic moment ($S=5/2$ in Sm, while it is 7/2 and 6/2 in Gd and Tb, respectively) and the resulting weakening of the effective magnetic exchange interactions. This finding is consistent with a recent report by Nirmala *et al.*[52] who showed that the monoclinic Dy_5Si_3Ge to orthorhombic Dy_5Si_3Ge transformation, which occurs around $T=50$ K on cooling, is only $\sim$50% complete (the spin magnetic moments of Sm and Dy are identical).

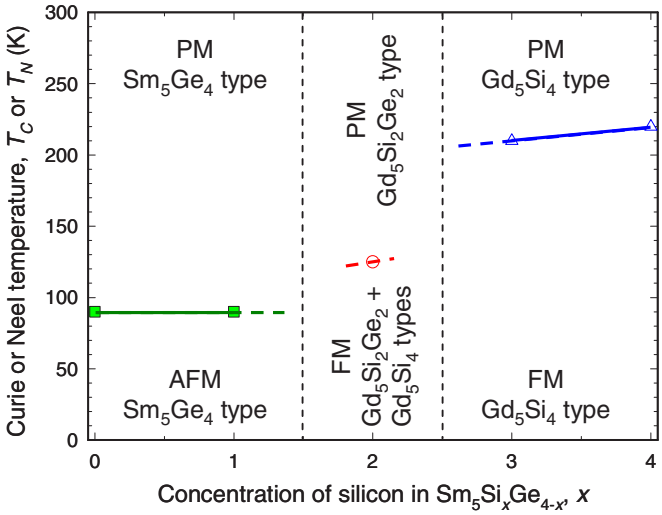

FIG. 14. (Color online) The tentative magnetic and crystallographic phase diagram of the $Sm_5Si_xGe_{4-x}$ system. Boundaries drawn using dashed lines are imprecise and should be considered as estimates only. Ferromagnetic $Sm_5Si_2Ge_2$ exists in a phase separated state adopting two different types of crystal structure, i.e., the monoclinic $Gd_5Si_2Ge_2$ and orthorhombic Gd_5Si_4 types.

The $Gd_5Si_2Ge_2$-type to Gd_5Si_4-type phase transformation begins at $T_{st}\cong 115$ K on cooling in a zero field, while the reverse transformation is completed at $T_{st}\cong 125$ K on heating. There is a difference of $\sim$10 K between the structural phase transformation on cooling and on heating in a zero magnetic field, which is consistent with that observed in the dc magnetic susceptibility in both ZFC and FC conditions for $Sm_5Si_2Ge_2$ (see Fig. 5). Moreover, $T_{st}\cong 125$ K on heating is nearly equal to the Curie temperature (125 K) determined from the heat capacity peak on heating in a zero magnetic field, which indicates that there is the coupling of the magnetic and crystallographic phase transitions in $Sm_5Si_2Ge_2$.

A tentative magnetic and crystallographic phase diagram of the $Sm_5Si_xGe_{4-x}$ system is shown in Fig. 14. Even though the diagram is preliminary, its similarity to those of the $Gd_5Si_xGe_{4-x}$ and $Tb_5Si_xGe_{4-x}$ systems is clear. We also note that this diagram is simpler than that of the $Tb_5Si_xGe_{4-x}$ system[18] because of the absence of spin-reorientation transitions. A magnetostructural phase transformation is only observed in the monoclinic phase region, because no ferro magnetic or ferrimagnetic state is reached in the Sm_5Ge_4-type phase region. Because this study is based on the examination of only five alloys, phase transition boundaries drawn using dashed lines should be considered only preliminary because their location may change when more data becomes available.

CONCLUSIONS

In summary, there are three distinct phase regions for $Sm_5Si_xGe_{4-x}$ alloys as x varies from 0 to 4, which are the Gd_5Si_4-type, the $Gd_5Si_2Ge_2$-type, and the Sm_5Ge_4-type structure; this behavior is consistent with the $Gd_5Si_xGe_{4-x}$ system. The unit cell dimensions of both Sm_5Si_4 and Sm_5Ge_4

compounds follow normal lanthanide contraction rule when compared to those of other lanthanides, thus indicating that Sm ions are in the trivalent state. The dc magnetic susceptibilities for $Sm_5Si_xGe_{4-x}$ alloys can be well described with the consideration of the temperature-independent Van Vleck term because of the narrow energy separation between $J=5/2$ and $J=7/2$ multiplet states of Sm^{3+} ions. The reduced effective magnetic moment and saturated magnetic moment of $Sm_5Si_xGe_{4-x}$ alloys are likely due to CEF splitting. The magnetic behaviors with the replacement of Ge by Si in $Sm_5Si_xGe_{4-x}$ alloys are similar to those observed in $Gd_5Si_xGe_{4-x}$ alloys (FM for Si-rich regions, first-order FM for intermediate regions, and AFM for Ge-rich regions). The magnetic transition temperatures of Sm_5Si_4 ($T_C=220$ K) and Sm_5Ge_4 ($T_N=90$ K) are higher than expected from de Gennes factor scaling in light lanthanide elements. An external magnetic field of 10 T does not suppress the heat capacity peaks, which are clearly of magnetic origin in the $Sm_5Si_xGe_{4-x}$ system, which is in contrast to the behavior observed in other $R_5Si_xGe_{4-x}$ systems such as when $R=$Gd or Tb, which are significantly affected (either reduced and broadened or shifted) by high magnetic fields. Thus, the magnetocaloric effect values are negligible in the $Sm_5Si_xGe_{4x}$ system. *In-situ* x-ray powder diffraction measurements as a function of temperature indicate that there is a coupling of the magnetic and structural phase transitions for $Sm_5Si_2Ge_2$.

ACKNOWLEDGMENTS

This work was supported by the Office of Basic Energy Sciences of the Office of Sciences of the U. S. Department of Energy under Contract No. DE-AC02-07CH11358 with Iowa State University of Science and Technology. The authors thank Ya. Mudryk for help with collecting temperature dependent x-ray powder diffraction data.

[1] G. S. Smith, A. G. Tharp, and Q. Johnson, Nature (London) **210**, 1148 (1966).
[2] G. S. Smith, Q. Johnson, and A. G. Tharp, Acta Crystallogr. **22**, 269 (1967).
[3] G. S. Smith, A. G. Tharp, and Q. Johnson, Acta Crystallogr. **22**, 940 (1967).
[4] F. Holtzberg, R. J. Gambino, and T. R. McGuire, J. Phys. Chem. Solids **28**, 2283 (1967).
[5] V. K. Pecharsky and K. A. Gschneidner, Jr., Phys. Rev. Lett. **78**, 4494 (1997).
[6] L. Morellon, P. A. Algarabel, M. R. Ibarra, J. Blasco, B. García-Landa, Z. Arnold, and F. Albertini, Phys. Rev. B **58**, R14721 (1998).
[7] L. Morellon, J. Stankiewicz, B. García-Landa, P. A. Algarabel, and M. R. Ibarra, Appl. Phys. Lett. **73**, 3462 (1998).
[8] V. K. Pecharsky and K. A. Gschneidner, Jr., Adv. Mater. (Weinheim, Ger.) **13**, 683 (1997).
[9] V. K. Pecharsky and K. A. Gschneidner, Jr., J. Alloys Compd. **260**, 98 (1997).
[10] V. K. Pecharsky and K. A. Gschneidner, Jr., Appl. Phys. Lett. **70**, 3299 (1997).
[11] W. Choe, V. K. Pecharsky, A. O. Pecharsky, K. A. Gschneidner, Jr., V. G. Young, Jr., and G. J. Miller, Phys. Rev. Lett. **84**, 4617 (2000).
[12] V. K. Pecharsky, A. O. Pecharsky, and K. A. Gschneidner, Jr., J. Alloys Compd. **344**, 362 (2002).
[13] W. Choe, A. O. Pecharsky, M. Worle, and G. J. Miller, Inorg. Chem. **42**, 8223 (2003).
[14] K. A. Gschneidner, Jr., V. K. Pecharsky, A. O. Pecharsky, V. V. Ivtchenko, and E. M. Levin, J. Alloys Compd. **303**, 214 (2000).
[15] H. F. Yang, G. H. Rao, W. G. Chu, G. Y. Liu, Z. W. Ouyang, and J. K. Liang, J. Alloys Compd. **339**, 189 (2002).
[16] H. F. Yang, G. H. Rao, G. Y. Liu, Z. W. Ouyang, W. F. Liu, X. M. Feng, W. G. Chu, and J. K. Liang, J. Alloys Compd. **346**, 190 (2002).
[17] A. O. Pecharsky, K. A. Gschneidner, Jr., V. K. Pecharsky, and C. E. Schindler, J. Alloys Compd. **338**, 126 (2002).
[18] C. Ritter, L. Morellon, P. A. Algarabel, C. Magen, and M. R. Ibarra, Phys. Rev. B **65**, 094405 (2002).
[19] A. O. Pecharsky, K. A. Gschneidner, Jr., V. K. Pecharsky, D. L. Schlagel, and T. A. Lograsso, Phys. Rev. B **70**, 144419 (2004).
[20] K. Ahn, A. O. Tsokol, Yu. Mozharivskyj, K. A. Gschneidner, Jr., and V. K. Pecharsky, Phys. Rev. B **72**, 054404 (2005).
[21] A. O. Pecharsky, V. K. Pecharsky, and K. A. Gschneidner, Jr., J. Alloys Compd. **379**, 127 (2004).
[22] M. V. Bulanova, P. N. Zheltov, K. A. Meleshevich, P. A. Saltykov, and G. Effenberg, J. Alloys Compd. **345**, 110 (2002).
[23] S. Bobev and E. D. Bauer, Acta Crystallogr., Sect. E: Struct. Rep. Online **61**, i73 (2005).
[24] L. M. Wu, S. H. Kim, and D. K. Seo, J. Am. Chem. Soc. **127**, 15682 (2005).
[25] P. Schobinger-Papamantellos and A. Niggli, J. Phys. (Paris), Colloq. **C5**, 156 (1979).
[26] V. N. Eremenko, V. E. Listovnichii, S. P. Lusan, Yu I. Buyanov, and P. S. Martsenyuk, J. Alloys Compd. **219**, 181 (1995).
[27] V. N. Eremenko, K. A. Meleshevich, Yu. I. Buyanov, and P. S. Martsenyuk, Sov. Powder Metall. Met. Ceram **28**, 543 (1989).
[28] N. P. Thuy, Y. Y. Chen, Y. D. Yao, C. R. Wang, S. H. Lin, J. C. Ho, T. P. Nguyen, P. D. Thang, J. C. P. Klaasse, N. T. Hien, and L. T. Tai, J. Magn. Magn. Mater. **262**, 432 (2003).
[29] Materials Preparation Center, Ames Laboratory US-DOE, Ames, IA, USA, www.mpc.ameslab.gov
[30] A. Desiredi, V. Piacente, and S. Nobili, J. Chem. Eng. Data **18**, 140 (1973).
[31] B. A. Hunter, Rietica-A visual Rietveld program. International Union of Crystallography Commission on Powder Diffraction, Newsletter No. 20 (Summer, 1998) http://www.rietica.org
[32] V. K. Pecharsky, A. P. Holm, K. A. Gschneidner, Jr., and R. Rink, Phys. Rev. Lett. **91**, 197204 (2003).
[33] Ya. Mudryk, A. P. Holm, K. A. Gschneidner, Jr., and V. K. Pecharsky, Phys. Rev. B **72**, 064442 (2005).
[34] A. P. Holm, V. K. Pecharsky, K. A. Gschneidner, Jr., R. Rink, and M. Jirmanus, Rev. Sci. Instrum. **75**, 1081 (2004).
[35] V. K. Pecharsky, J. O. Moorman, and K. A. Gschneidner, Jr., Rev.

Sci. Instrum. **68**, 4196 (1997).
[36] N. W. Ashcroft and N. D. Mermin, *Solid State Physics* (Holt, Reinhart and Winston, New York, 1976).
[37] J. H. Van Vleck, *The Theory of Electric and Magnetic Susceptibilities* (Oxford University Press, London, 1932).
[38] A. Frank, Phys. Rev. **48**, 765 (1935).
[39] H. W. De Wijn, A. M. Van Diepen, and K. H. J. Buschow, Phys. Rev. **161**, 253 (1967).
[40] A. M. Stewart, Phys. Rev. B **6**, 1985 (1972).
[41] Z. Liu, Phys. Rev. B **64**, 144407 (2001).
[42] H. Adachi, H. Ino, and H. Miwa, Phys. Rev. B **56**, 349 (1997).
[43] H. Adachi, H. Ino, and H. Miwa, Phys. Rev. B **59**, 11445 (1997).
[44] H. Adachi and H. Ino, Nature (London) **401**, 148 (1999).
[45] H. Adachi, H. Kawata, H. Hashimoto, Y. Sato, I. Matsumoto, and Y. Tanaka, Phys. Rev. Lett. **87**, 127202 (2001).
[46] D. Wagner, *Introduction to Theory of Magnetism* (Pergamon, Oxford, 1972).
[47] H. C. Hamaker, L. D. Woolf, H. B. MacKay, Z. Fisk, and M. B. Maple, Solid State Commun. **32**, 289 (1979).
[48] W. M. Yuhasz, N. A. Frederick, P.-C. Ho, N. P. Butch, B. J. Taylor, T. A. Sayles, M. B. Maple, J. B. Betts, A. H. Lacerda, P. Rogl, and G. Giester, Phys. Rev. B **71**, 104402 (2005).
[49] V. K. Pecharsky and K. A. Gschneidner, Jr., J. Appl. Phys. **86**, 565 (1999).
[50] V. K. Pecharsky and K. A. Gschneidner, Jr., in *Magnetism and Structure in Functional Materials*, edited by A. Planes, L. Mañosa, and A. Saxena (Springer-Verlag, Berlin, 2005), Chap. 11, p. 199.
[51] M. Zou, Ya. Mudryk, V. K. Pecharsky, K. A. Gschneidner, Jr., D. L. Schlagel, and T. A. Lograsso, Phys. Rev. B **75**, 024418 (2007).
[52] R. Nirmala, Ya. Mudryk, V. K. Pecharsky, and K. A. Gschneidner, Jr. (unpublished).